Preparation and characterization of graphene oxide-based nanocomposite materials for solar energy sorption

Thuy Thi Le Bui, Ngoc Cong Pham, Thao Dinh Pham & Linh Thi Nguyen

Chemical Papers

ISSN 2585-7290

Chem. Pap.
DOI 10.1007/s11696-020-01455-0

Springer

Chemical Papers
https://doi.org/10.1007/s11696-020-01455-0

ORIGINAL PAPER

Preparation and characterization of graphene oxide-based nanocomposite materials for solar energy sorption

Thuy Thi Le Bui[1] · Ngoc Cong Pham[2] · Thao Dinh Pham[1] · Linh Thi Nguyen[1]

Received: 23 July 2020 / Accepted: 25 November 2020

Abstract

Two series of nanocomposite materials based on graphene oxide (GO) (Al_2O_3/GO (Al/GO), Fe_3O_4/GO (Fe/GO), and Fe_3O_4–Al_2O_3/GO (Fe–Al/GO)), and reduced graphene oxide (rGO) (Al_2O_3/rGO (Al/GO), Fe_3O_4/rGO (Fe/GO), and Fe_3O_4–Al_2O_3/rGO (Fe–Al/rGO)) were prepared and characterized by X-ray and infrared spectra, SEM, TEM and EDX analyses. Graphene oxide was synthesized from graphite by improved Hummers method, then it was reduced by ascorbic acid to obtain rGO. Composite materials were prepared by suspension mixing. GO- and rGO-based materials were dispersed into brine water to form nanofluids. Transmittance spectra and thermal conductivity of nanofluids and reflectance spectra of the three-component composites were systematically investigated to evaluate their thermal sorption capacity. It can be seen from the transmittance spectra that nanofluids capture almost incident light and from the reflectance that synthesized materials absorbed more than 97.5% and 96% of the irradiated solar power. The thermal conductivity results show that hybrid nanofluid showed high thermal conductivity than single nanofluids. The thermal absorption ability of nanofluids was evaluated by change in temperatures and weights of nanofluids. Results showed that all prepared materials (either single form such as GO, rGO, Al_2O_3 or composite form such as Al/GO, Fe/GO, Fe–Al/GO, Al/rGO, Fe/rGO, Fe–Al/rGO) raised thermal sorption of brine water. The combination of two or three components leaded to higher thermal sorption ability. Fe–Al/GO and Fe–Al/rGO give the highest thermal absorption efficiency (the temperature difference between the blank sample and the sample containing material with content of 0.5 mg mL^{-1} is 7 °C and 8.5 °C, respectively). Evaporation ability of Fe–Al/GO and Fe–Al/rGO nanofluids increased to 67% and 79%, respectively. The thermal sorption increased with increasing the concentration of materials in nanofluid and lightening intensity (the temperature difference between the blank sample and investigated sample using two lamps was 21 °C). Moreover, 98% of Fe–Al/GO (Fe–Al/rGO) was simply recovered by magnet and the recovered material can be reused with only slight decrease in thermal sorption performance. Prepared nanocomposite was dispersed in brine water (0.15 mg mL^{-1} in 3.5% NaCl solution) to be distillated using solar energy and the results show that distillation process can be profoundly speeded up.

Keywords Graphene oxide · Reduced graphene oxide · Solar thermal sorption · Nanocomposite · Magnetic property · Distilling brine water

Introduction

The exhaustion of portable water is a global problem that most countries in the world have been facing while seawater covers three fourth of the Earth and could be utilized for drinking and for use in some industries after desalination. Numerous methods are used for water purification such as filtration, disinfection, sedimentation, and distillation (Alharahsheh et al. 2018). To utilize the available solar energy to reduce costs, water distillation technique using solar energy has been studied and used for a long time (solar distillation process). In this technique, a solar still is used

✉ Thuy Thi Le Bui
thuykhai2001@gmail.com

[1] Oil Refinery and Petrochemistry Department, Hanoi University of Mining and Geology, 18-Vien, Duc Thang, Bac Tu Liem, Ha Noi, Viet Nam

[2] High School for Gifted Students, Hanoi National University of Education, 136 Xuan Thuy, Dich Vong Hau, Cau Giay, Ha Noi, Viet Nam

Published online: 10 January 2021

to produce potable water. The main disadvantage of this technique is the waste of much solar energy because water absorbs only 13% of the radiant energy.

An effective method is to disperse nanomaterials that can enhance the efficiency of thermal absorption into liquid media: water, glycol, oil, etc. to form nanofluids (Raj and Subudhi 2018; Sarsam et al. 2015; Syam Sundara et al. 2017; Malega et al. 2018; Omid et al. 2017; El-Said et al. 2015). Nanoparticles of some metals (Cu, Ag, Au, Ni), metal oxides (Al_2O_3, Cu_2O, TiO_2, etc.), and carbon forms (carbon nanotubes, graphene oxide, etc.) have been dispersed in water to increase thermal sorption efficiency of water, for example, the thermal sorption efficiency of a saline aqueous suspension that contained 0.1% of Al_2O_3 is 29.95% higher than that of brine water (Elango et al. 2015). In another report, CuO, Al_2O_3 and TiO_2 nanoparticles were also used in solar stills to collect fresh water; the evaporation efficiency increased up to 50% compared to saline water (Madhu et al. 2017). However, such thermal sorption efficiency is not high enough to commercialize widely the solar still. Moreover, in the actual seawater distillation devices, after collecting fresh water, the concentrated salty solution needs to be removed, if the nanoparticles are directly dispersed into the distillation flask, then separation and recovery of nanoparticles from the salty solution could be difficult.

To further improve thermal absorption efficiency, recent scientists have focused on the use of carbon-based materials (graphite, graphene, graphene oxide, carbon nanotubes, etc.), which are considered as good thermal sorption followed blackbody theory (thermal conductivity 5000 W m^{-1} K^{-1}) (Madhu et al. 2017). Carbon nanotubes, graphene, graphene oxide were used as materials for direct thermal absorption in solar distillation process of sea water; all of them showed high thermal sorption effectiveness and graphene showed the highest effectiveness (Mahmudul et al. 2015). However, these materials are quite expensive and difficult to be recovered so that their application is limited. Wang et al. (2016) developed a solar thermal evaporation system based on reduced graphene oxide (rGO) decorated with magnetic nanoparticles and reported that this material can absorb highly sunlight and it could be separated from seawater under the action of magnetic force by decorated with magnetic nanoparticles. Furthermore, some studies have shown that nanocomposites (hybrid nanoparticles) have higher thermal sorption efficiency than single nanomaterials (Syam Sundara et al. 2017). A great number of nanocomposites (hybrid nanoparticles) have been introduced into the liquid to form nanofluids and have been shown to have higher thermal sorption ability than single nanoparticles (El-Sawy 2017; El-Said et al. 2016; Ojeda and Messina 2017; Chen et al. 2019).

The high thermal sorption efficiency of nanocomposite materials was also shown by the thermal conductivity; an important factor governs the thermal sorption ability of materials. In recent decades, numerous experimental works have been conducted to investigate the thermal properties of metal oxides (CuO, Al_2O_3, TiO_2, etc.) nanofluids and hybrid nanofluids (Manimaran et al. 2014; Patel et al. 2010; Syam Sundar et al. 2013; Irnie Zakaria et al. 2015; Suresh et al. 2012; Selvakumar Suresh 2012, Madhesh et al. 2014). Thermal characteristics of water-based Al_2O_3–MWCNT hybrid nanofluids with different weight concentrations were investigated by Nine et al. (2012). The experimental results showed that the thermal conductivity of hybrid nanofluids with spherical nanoparticles was higher than that of nanofluids with single nanoparticles. Thermal conductivity enhancements of some nanofluids followed the order water < Al_2O_3/water < CuO/water < Al_2O_3-–CuO/water nanofluids (Senthilraja 2015).

Therefore, it was the subject of this work to prepare nanocomposites based on graphene (or graphene oxide), Al_2O_3 nanoparticles, and magnetic compounds (Fe_3O_4) for high thermal sorption and for reducing high cost and secondary pollution. The optical properties, thermal conductivity, thermal sorption, and reusability of materials were investigated systematically.

Materials and methods

Materials

Graphite (99%) was supplied by Sigma-Aldrich; H_2SO_4 (98%), $KMnO_4$ (99%), H_2O_2 (30%), $FeCl_3.6H_2O$ (99%), HCl (36–38%), $NaNO_3$ (99%), $FeSO_4.7H_2O$ (99%), $AlCl_3.6H_2O$, ethanol (99.7%), ascorbic acid (99.9%), citric acid (99%), polyvinyl chloride (PVA), and NH_3 (25%) were provided by Guangdong Guanghua, China.

Synthesis of nanocomposite materials

The synthesis processes of all the materials were referred to the methods in cited documents but with small modifications (in most situation, the materials were kept in the solution for further steps without drying and grinding) to create materials of small dimensions.

Preparation of GO using modified Hummers' method (Hummer and Offerman 1958; Shahriary and Athawale 2014; Alibeyli et al. 2014)

5 g of graphite and 2.5 g of $NaNO_3$ were gradually added to a cold H_2SO_4 solution (115 mL, 98%) prepared at 5 °C in an ice bath and stirred by a magnetic stirrer for 5 min. Then, the mixture was stirred by a magnetic stirrer for 30 min and then 15 g of $KMnO_4$ was added slowly in 15 min. During

the addition, suspension's temperature was kept below 15–18 °C. Once mixed, the suspension was transferred to a 35 ± 5 °C water bath and stirred for about 30 min; then, 230 mL of distilled water was added slowly to the reaction beaker to keep the temperature at around 44–48 °C. Once added, the temperature was increased to 90 °C and the suspension was stirred for extra 15 min at this temperature. Finally, 500 mL of water containing 30 mL of H_2O_2 was added to the suspension. High-concentrated HCl solution was added to the final suspension to accelerate precipitation. The solid content of final suspension was precipitated by centrifugation with 9000 rpm in 5 min. Then, for purifying from SO_4^{2-}, the precipitants were dispersed in HCl (3.7%) and stirred for 15 min. Then, the centrifugation was applied again at 9000 rpm. This purification processwas repeated until no SO_4^{2-} ion detected by $BaCl_2$. GO was stored in 500 ml of distilled water.

Preparation of rGO (Kanishka et al. 2018; Rogojan et al. 2011)

One g of GO was dispersed in 300 ml of distilled water by ultrasonic generator for one hour to form a suspension. Suspension was stirred and the temperature was gradually raised to 50 °C. Then, 10 g of ascorbic acid was slowly added during 2 h and stirred for 8 h at 50 °C. The suspension was centrifuged and washed several times with acetone. Then, the acetone solution containing GO was added into 50 mL of deionized water. The resulting solution was heated at 65 °C while being stirred for another 2 h to evaporate the acetone. The obtained product was reduced graphene oxide (rGO).

Preparation of Al/GO and Al/rGO (Varghese and Hariharan 2014; Bartolucci et al. 2011)

25% ammonia solution was added to 200 mL of 0.1M alcoholic $AlCl_3$ solution until pH of 9. The resulting solution turned to a white sol. Next, 150 mL of PVA (0.5%) aqueous solution was added and the mixture was stirred continuously using a magnetic stirrer. The obtained gel was allowed to mature for 24 h at room temperature and treated at 100 °C for another 24 h which leads to the formation of light-weight porous materials due to the enormous gas evolution. Finally, the dried gel was calcined at 800 °C for 4 h and the calcined powders were crushed using mortar and pestle to get the fine homogeneous dense powder (Varghese and Hariharan 2014).

To prepare Al/GO (or Al/rGO) nanocomposite material, 200 mL of aqueous suspension containing 0.1 g of GO (or rGO) was ultrasonicated for one hour. Then 0.1 g of Al_2O_3 nanoparticles was added to the suspension, the mixture was ultrsonicated for 20 min and stirred for 6 h. The resulting product was denoted as Al/GO (or Al/rGO).

Preparation of Fe/GO and Fe/rGO; Fe–Al/GO and Fe–Al/rGO

Fe_3O_4 nanoparticles (Stankovich 2007; Xiangqing Wang et al. 2016) 3.03 g of $FeCl_3.6H_2O$ and 1.56 g of $FeSO_4.7H_2O$ were dissolved in 150 mL of distilled water and the mixture was stirred by magnetic stirrer for 30 min to form a bright yellow solution. 25% NH_3 solution was added until pH of 10 and then stirred for 30 min. 1 g of citric acid monohydrate was introduced to increase the dispersity of the solution. Once the reaction was completed, the black precipitation was collected with a magnet, then washed several times with water and acetone to pH = 7. Then, the acetone solution containing the nanoparticles was added into 50 mL of deionized water. The resulting solution was heated at 65 °C while being stirred for another 2 h to evaporate the acetone.

Fe/GO and Fe/rGO nanomaterials (Stankovich 2007; Xiangqing Wang et al. 2016) 300 mL of a suspension containing 0.3 g of GO (or rGO) was ultrasonicated for 30 min to form a homogeneous GO (or rGO) suspension. Then, a suspension containing 0.3 g Fe_3O_4 nanoparticles was added in and the mixture was ultrasonicated for 30 min to get homogeneous suspension. This suspension was stirred for 6 h more. Fe/GO (Fe/rGO) was kept in water for further uses.

Fe–Al/GO and Fe–Al/rGO nanomaterials The procedures similar to the above were repeated. 300 mL of suspension containing 0.3 g of Al/GO (or Al/rGO) was ultrasonicated for 30 min to form a homogeneous Al/GO (or Al/rGO) suspension. Then, a suspension containing 0.15 g Fe_3O_4 nanoparticles was added in and the mixture was ultrasonicated for 30 min to get homogeneous suspension. Finally, this was followed by stirring for 6 h. Fe–Al/GO (Fe–Al/rGO) was kept in water for further uses.

Evaluation of thermal sorption capacity of materials

Different amounts of materials were added into 200 mL of 3.5% NaCl aqueous solutions in 250 ml beakers. The outer surface of the beaker's wall was covered by an insulation coating. The beaker was radiated by a Metal Halide Philips lamp (MH-150W E27) (Tawfik 2018). The temperature of each sample was measured and recorded every 10 or 15 min by a OEM TM-902C thermal couple (accuracy of 0.1 degree) and high-precision electronic scales (Kern ALJ 250-4A) were employed to monitor the mass loss of bulk liquid during solar illumination to evaluate the evaporation efficiency with the accuracy of 0.001 g.

Recoverability test of materials: After thermal adsorption experiments, materials were recovered with a magnet and rinsed with demineralized water until no chloride ion was detected. Then, the recovered material was weighted to calculate recovery yield and measured FT-IR spectra.

Reusability tests of materials: Recovered materials were re-dispersed in 3.5% NaCl aqueous solutions to form nanofluid and used for thermal sorption experiments.

Characterization of materials

X-ray spectra of materials were performed using D8 Advance Bruker; SEM of materials was measured by Joel 6490 JED-2300; and TEM of materials was measured by Jeol-1010. EDX of materials was conducted by JED-2300—JEOL and FT-IR of materials was measured using (4600 JASCO). The reflectance spectra were collected via Cary 5000 UV–Vis–NIR (Aglient-Technologies); the transmittance of nanofluids was measured by Shimadzu UV-2600, Japan (1400–220 nm). Thermal conductivity of nanofluids was measured using Flucon Lambda (Flucon Fluid Control GmbH, Germany).

Results and discussion

Characterization of materials

FT-IR spectra

FT-IR spectra of synthesized materials are given in Fig. 1. As seen in GO spectrum, the peak of wave numbers of 3480 cm^{-1} and 1400 cm^{-1} shows the vibration and deformation of the O–H groups, respectively (Senthilrajaa et al. 2015). The bands at wave numbers of 1692 cm^{-1}, 1572 cm^{-1}, 1258 cm^{-1}, and 1062 cm^{-1} are typical absorption of C=O, C=C, C–OH and C–O (alkoxy) groups. These illustrate the presence of oxygen functional groups in GO. These results are consistent with the findings of (Kanishka et al. 2018; Shahriary and Athawale 2014). Infrared spectrum of Al_2O_3 showed all its typical peaks. The oscillation of the O–H group is shown by a peak of wave numbers of 3487 cm^{-1}. The band at 1636 cm^{-1} is due to the O–H group of H–O–H; the typical vibration of Al–O and Al–O–Al group is shown by a broad band of wave number of 600 cm^{-1} – 800 cm^{-1}(Rogojan et al. 2011). The band at wave number of 571 cm^{-1} is due to the stretching vibration of the Fe–O functional group. The number of waves in the range 1625 cm^{-1}–1400 cm^{-1} indicates the presence of bending vibration of the H–O–H group, while the O–H group has the oscillations at about 3380 cm^{-1} (Malega et al. 2018, Omid et al. 2017).

From the spectra of GO, Al_2O_3, and Al/GO it can be seen that the infrared spectrum of Al/GO has almost characteristic peaks of GO and Al_2O_3 (Fig. 1); however, the intense peaks of GO (at 1692 cm^{-1}, 1572 cm^{-1}, 1258 cm^{-1} and 1062 cm^{-1} of the functional groups C=O, C=C, C–OH and C=O) are reduced due to a decreased concentration of GO. Similarly, all the typical bands of the GO and Fe_3O_4 FT-IR spectrum are observed in Fe/GO spectra but with reduced intensity due to decreased GO concentration.

The FT-IR spectra results of GO, Al/GO, Fe/GO, and Fe–Al/GO show that the nanocomposite materials have all of characteristic peaks of individual materials but with reduced intensity.

Figure 2 compares the functional group of rGO, Al/rGO, Fe/rGO, and Fe–Al/rGO using FT-IR spectrometer. As seen from the figure that rGO contains a few oxygenated functional groups with awide boad (O–H stretching

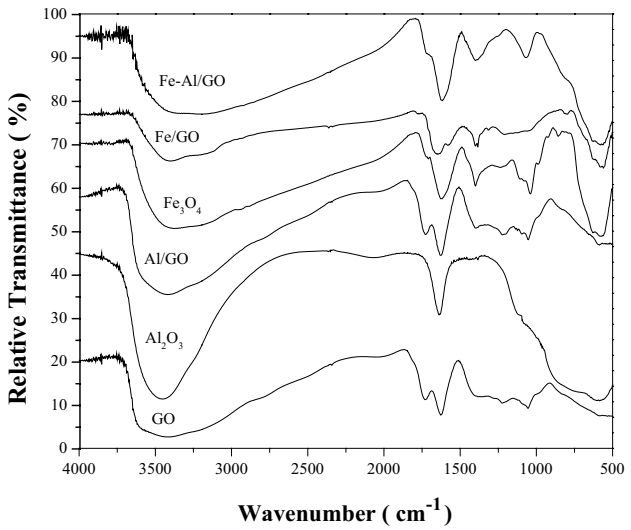

Fig. 1 FT-IR of GO and nanocomposites based on GO, Al_2O_3, and Fe_3O_4

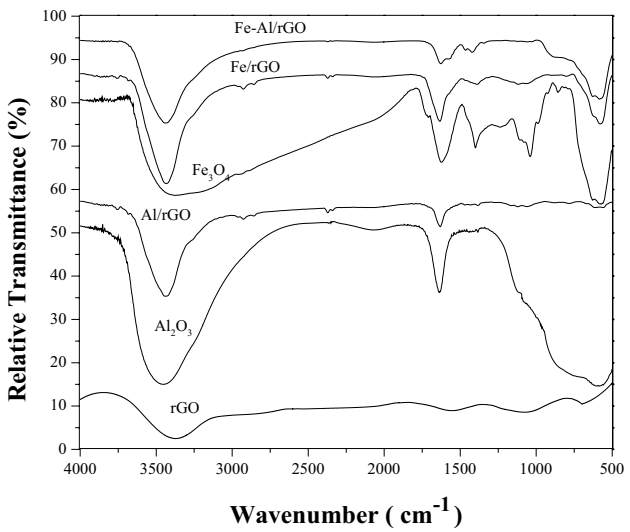

Fig. 2 FT-IR of rGO and nanocomposites based on rGO, Al_2O_3, and Fe_3O_4

vibration) at 3300 cm^{-1} to 3700 cm^{-1} and weak board (C=C and –C=O stretching vibration) at 1450 cm^{-1} to 1650 cm^{-1}, respectively, and weal peak (–C–O– stretching vibration) at 1250 cm^{-1}). This means that almost oxygenated functional groups were reduced by ascorbic acid (Malega et al. 2018).

It can be seen from the spectra of rGO, Al_2O_3, and Al/rGO that the infrared spectrum of Al/rGO has almost characteristic peaks of rGO and Al_2O_3 (Fig. 2), for example, the moderate intense board (3300–3700 cm^{-1}) shows the presence OH group in rGO and Al_2O_3; while, the peak at 1636 cm^{-1} is due to the O–H group of H–O–H in Al_2O_3.

Similarly, Fe/rGO and Fe–Al/rGO have all of the characteristic peaks of individual materials but with reduced intensity.

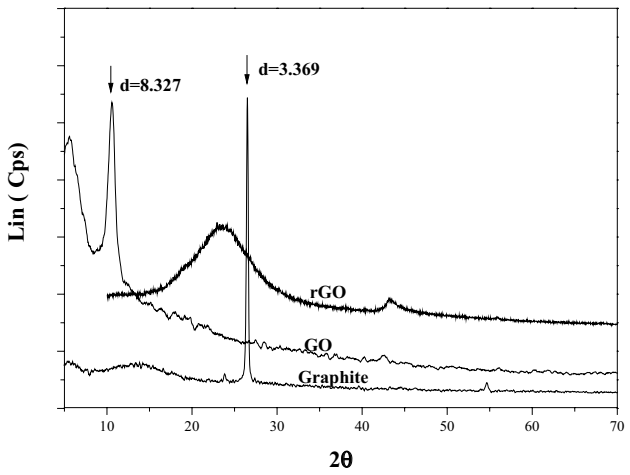

Fig. 3 X-ray diffraction of graphite, GO, and rGO

X-ray diffraction of materials

It can be seen in the X-ray diffraction (Fig. 3) that graphite has crystallinity morphology and large crystalline size due to a high intensity and sharp peak at 2θ = 26.5° (with interlayer space is 3.369 Å). When graphite was exposed to $KMnO_4$/H_2SO_4, the graphitic interlayer space will increase and bond between layers is weakened. When GO was formed, the peak at 2θ = 26.5° disappeared and a new peak appeared at 2θ = 11.2°. The interlayer spacing increases from 3.369 Å in graphite to 8.327 Å in graphene oxide. This is due to the formation of abundant oxygen-containing functional groups (–OH, –COOH, –O–, –CO–, etc.) on both sites of the sheet during oxidation. When GO was reduced to rGO by ascorbic acid, the number of those groups decreased. rGO is characterized by an intense and broad peak at 2θ = 24.5° and weak peak at 2θ° = 44. The intense and broad peak shows the amorphous crystallite particles of rGO. The interlayer spacing decreased due to effectiveness in removal oxygenated functional groups. This result is consistent with the results obtained from the previous studies (Alibeyli et al. 2014; Zainuddin et al. 2018).

It can be seen from XRD results (Fig. 4a) of Fe–Al/GO that the addition of Al_2O_3 and Fe_3O_4 results in the decrease in typical peak of GO at 2θ = 11.2° and the appearance of some new peaks at 2θ = 37°; 2θ = 45.6°; and 2θ = 67.1° corresponding to XRD data of γ-Al_2O_3 and 2θ = 30.23°; 2θ = 35.69°; 2θ = 57.41°; 2θ = 62.87° corresponding to XRD data of Fe_3O_4 (Syam Sundar et al. 2017; Elango et al. 2015). The similar results in XRD of Fe–Al/rGO were also observed. The decrease in typical peaks of GO and rGO (2θ = 11.2° and 2θ = 24.5°) indicates that the GO and rGO

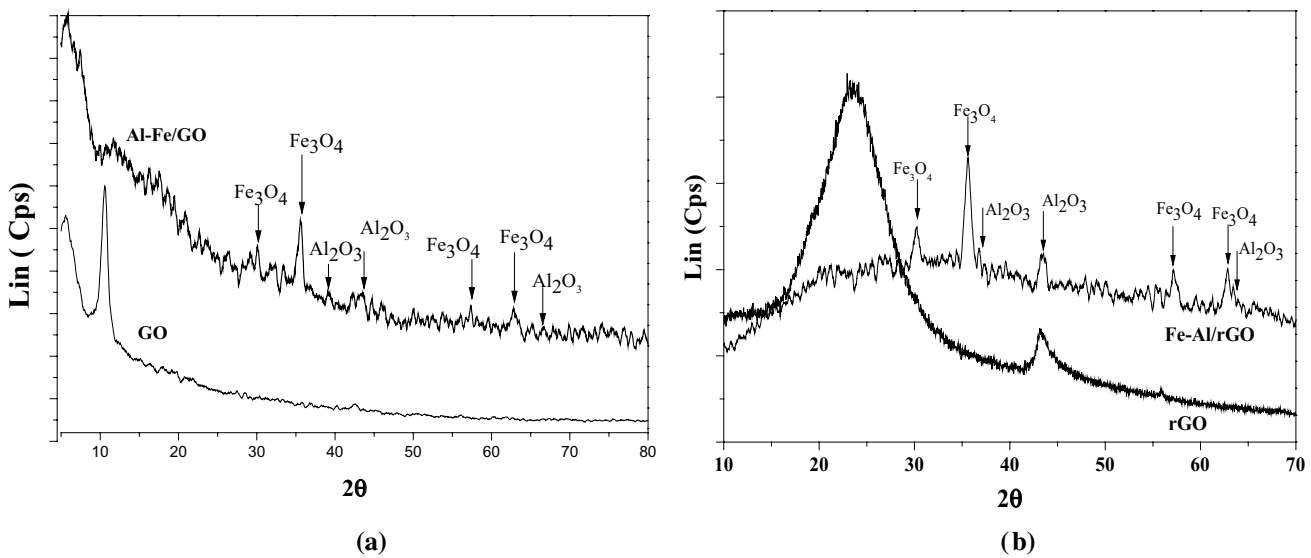

Fig. 4 XRD of GO and Al–Fe/GO (**a**); rGO and Al–Fe/rGO (**b**)

layers have been separated by the combination with Fe_3O_4 and Al_2O_3 nanoparticles during the preparation processes.

SEM, TEM, and EDX results

It can be seen from SEM and TEM images of Fe–Al/GO and Fe–Al/rGO materials (Figs. 5 and 6) that Al_2O_3 and Fe_3O_4 particles have spherical shape with diameters 8–10 nm dispersed on the surface of GO and rGO layers. The stability of Al_2O_3 and Fe_3O_4 on the surface of GO and rGO can be due to the static attraction of Al_2O_3 and Fe_3O_4 with oxygenated functional groups (–OH, –O–, –C = O, –COOH) on GO and rGO layers or the interaction of functional groups on the oxide surface (–OH) can with the groups on the surface layers of GO and rGO (–COOH, –OH, etc.) (Anum Iqbal et al. 2018; Hu et al. 2015), for example:

$$Al_2O_3\text{–}OH + rGO\text{–}COOH \rightarrow Al_2O_3\text{–}OCO\text{–}rGO + H_2O.$$

The good combination of three-member composite material was also observed when 98% of used composite material can be recovered with magnets (Sect. 3.3).

EDX analysis data (Table 1) showed that Fe–Al/GO (Fe–Al/rGO) contains 4 elements C, O, Al and Fe (from three components: Fe_3O_4, Al_2O_3, and GO (rGO)). Oxygen atoms exist mainly in Al_2O_3, Fe_3O_4, and functional groups (–C=O, –COOH, etc.) on the surface of GO (rGO). The content of O in Fe–Al/rGO is lower than in Fe–Al/GO because most of the oxygen-containing groups in GO were reduced during the preparation of rGO.

Optical properties of materials

The solar radiation harvesting capacity of nanofluids is the major factor that affects the utilization of solar energy and vapor generation. In this work, the transmittance of nanofluids containing studied materials and reflectance of some

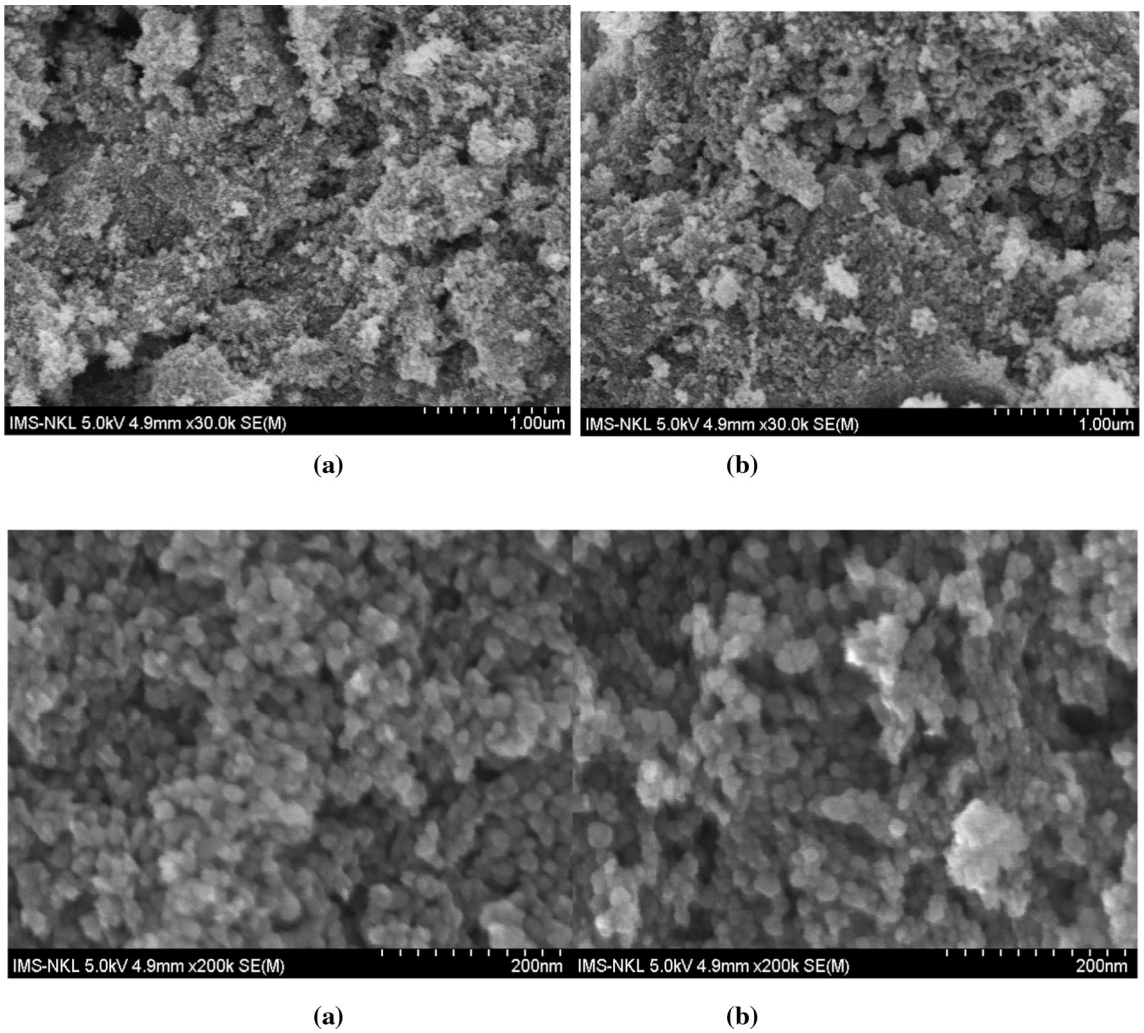

Fig. 5 SEM images of (**a**) Fe–Al/GO and (**b**) Fe–Al/rGO

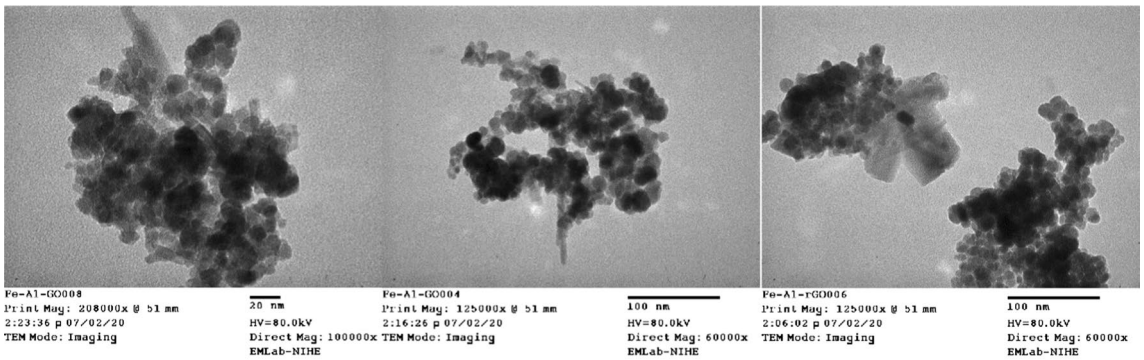

Fig. 6 TEM images of Fe–Al/GO (**a**, **b**) and (**c**) Fe–Al/rGO

Table 1 EDX results of Fe–Al/GO and Fe–Al/rGO

Elements	Fe–Al/GO		Fe–Al/rGO	
	Weight composition (%)	Elemental composition (%)	Weigh composition (%)	Elemental composition (%)
C	34.40	45.94	44.02	56.51
O	45.79	45.86	37.07	35.37
Al	8.41	4.99	8.66	4.95
Fe	11.40	3.26	10.26	2.83
Total	100	100	100	100

materials were measured. Transmittance of nanofluids based on GO and rGO is presented in Fig. 7.

The transmittance of nanofluids depends on the darkness of nanoparticles in fluids. In GO series, at the same concentration, GO showed the lowest transmittance and could capture nearly 100% incident light. When GO is combined with Fe_3O_4 the darkness decreases; therefore, the transmittance of Fe/GO reduces corresponding. Al_2O_3 has light gray color and results in the decrease in transmittance of its material-based nanofluids. The higher the content of Al_2O_3 in materials, the lower the transmittance of their nanofluids. rGO has a higher darkness than GO and also captures 100% incident light; the rGO-based materials have higher transmittances than GO-based ones, respectively.

The light absorbance and transmittance (absorbance = 2-log (%T)) of three-component material nanofluids (with brine water as control substance) with different concentrations are shown in Fig. 8.

According to the results shown in Fig. 8a, it appears that the magnetic nanofluids have broader absorption band in the visible light and the short wave of near infrared range from 200 to 1400 nm. Compared to brine water, the GO- and rGO-based nanoparticles could extend the solar

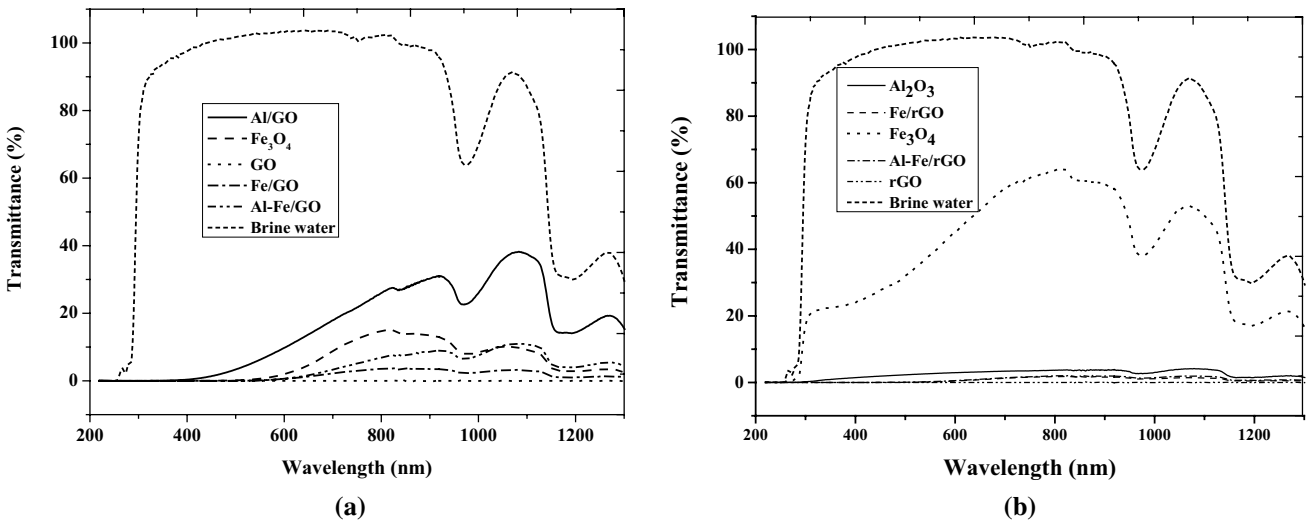

Fig. 7 Transmittance of nanofluids of (**a**) GO-based materials and (**b**) rGO-based materials at 0.15 mg mL^{-1} in 3.5% NaCl aqueous solution

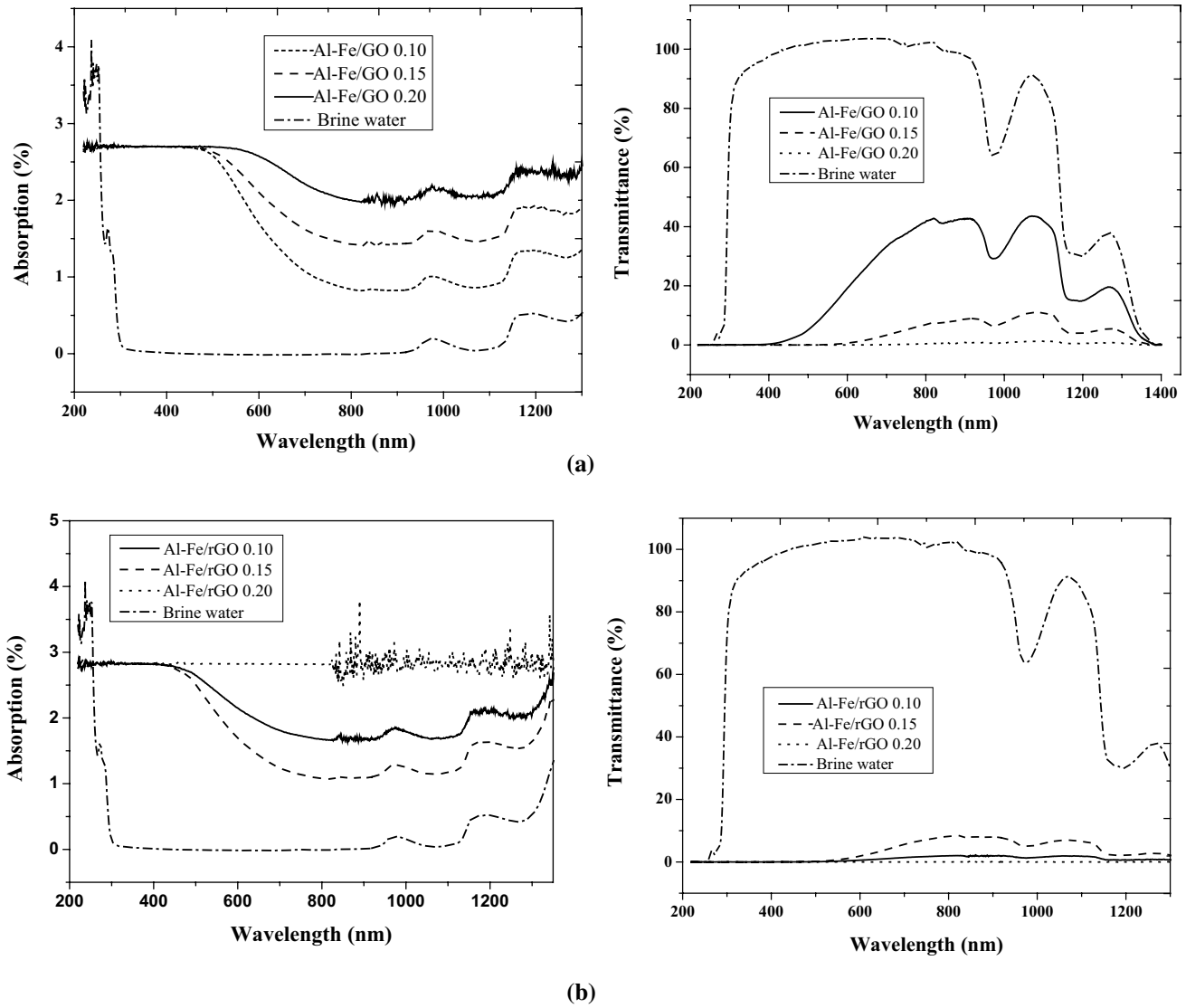

Fig. 8 The absorbance and transmittance of Fe–Al/GO (**a**) and Fe–Al/rGO (**b**) nanofluids at different concentrations

energy absorption capacity of brine water. The absorbance increased with increasing the nanoparticle concentration from 0.2 mg mL^{-1} to 1.5 mg mL^{-1} (0.02–0.15%) and the transmittance reduced conversely. Similar results were observed with recoverable carbon nanotube nanofluids (Chen et al. 2019). The transmittance of nanofluid showed that all magnetic nanofluids have lower transmittance than water. The nanofluid could capture nearly 90% of incident light at nanoparticle concentration of 0.15 mg mL^{-1} and nearly 100% at concentration of 0.2 mg mL^{-1}. Especially, when the concentration of nanoparticles is above 0.2 mg mL^{-1}, the whole of light from 200 to 1400 nm cannot cross nanofluids. It could be attributed to the direct photon absorbing and scattering phenomenon by nanoparticles. Similar to the results obtained from the experiments of evaluation of the thermal sorption capacity of materials (Sect. 3.2), Fe–Al/rGO nanofluids show higher absorbance and lower transmittance than Fe–Al/GO ones.

The reflectance (Fig. 9) spectrum shows that the reflectance of Fe–Al/GO and Fe–Al/rGO is below 4% and 2.5%, respectively, in the wavelength range of 220–2000 nm. Thus, more than 97.5% and 96% of the irradiated solar power are absorbed by the magnetic materials. The spectrum indicates a better solar absorption of Fe–Al/rGO compared with Fe–Al/GO due to the higher light absorption capacity of rGO compared with GO.

Thermal conductivity of materials

Besides the optical properties mentioned above, thermal conductivity also is an important property because absorbed irradiation solar power needs to be transferred to water to

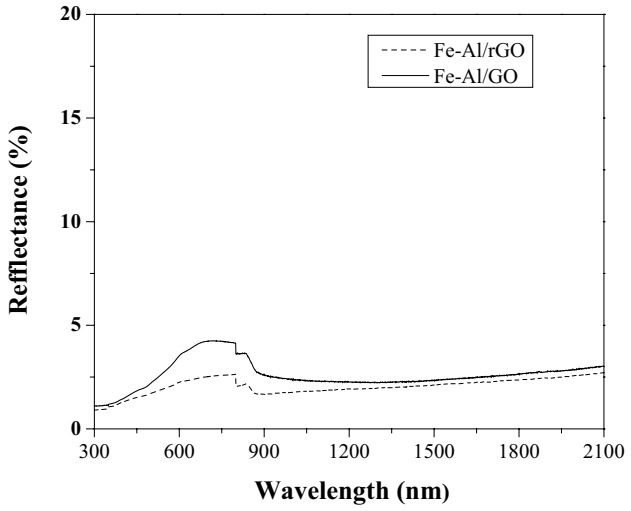

Fig. 9 The reflectance of Fe–Al/GO and Fe–Al/rGO materials

raise the temperature and volatility of brine water. When irradiation solar power absorbed is transferred to medium (water), then the thermal sorption capacity of materials increases. The Eq. (1) was used to calculate the thermal conductivity enhancements of nanofluids (Senthilraja et al. 2015).

$$\%K = \left[\frac{K_{nf} - K_{bf}}{K_{bf}}\right] \times 100, \tag{1}$$

where: K : is thermal conductivity enhancements of nanofluids; K_{nf}: thermal conductivity of nanofluid dispersed nanomaterials (mW m^{-1} K^{-1}); K_{bf}: thermal conductivity of brine water 3.5% as blank fluid (mW m^{-1} K^{-1}).

The variations of thermal conductivity enhancements with temperatures of nanofluids dispersed GO- and rGO-based materials are presented in Fig. 10. It can be seen that the thermal conductivity of nanofluids strongly depends on some factors such as structure of materials used to prepare nanofluids and temperature of nanofluids (Hu et al. 2015; Hojjat et al. 2010).

The influence of temperature on thermal conductivity enhancement of different nanofluids and the brine water was measured within the range of 30°–60 °C. It can be understood that the thermal conductivity enhancement of all nanofluids linearly increased with increasing temperature. Similar cases were reported previously for different nanofluids (Senthilraja et al. 2015). For all nanofluids in investigated temperature range, the maximum thermal conductivity enhancement was obtained at 60 °C. The thermal conductivity was enhanced from 16 to 44% and 18 to 49% for Fe–Al/GO/water and Fe–Al/rGO/water nanofluids at 0.15 mg mL^{-1} concentration, respectively. At higher temperatures, Brownian motion and collisions between nanoparticles in base fluids increased which resulted in the enhancements of thermal conductivity (Botha et al. 2011).

The experimental results clearly showed that GO has lower thermal conductivity enhancement than rGO. It can be due to some sp^2 hybridized carbon atoms of graphite were converted to sp^3 hybridized ones during the oxidation of graphite to form oxygen functional groups in GO. Most of these oxygen functional groups in GO were reduced during reduction of GO to rGO and sp^3 hybridized carbon atoms were converted back again to sp^2 ones. This makes rGO as currently one of the best conductive materials (Chen et al. 2019). Similarly, the nanofluids of rGO-based materials have higher thermal conductivity enhancement than nanofluids of GO-based materials.

The experimental results showed that the hybrid nanofluids have higher thermal conductivity enhancement than single nanofluids. To compare the thermal conductivities of four kinds of nanofluid prepared from four single materials, Al_2O_3, Fe_3O_4, GO, and rGO were measured. The thermal conductivities of single material nanofluids followed the order $Al_2O_3 < GO < Fe_3O_4 < rGO$. The two-component materials Al/GO, Fe/GO, Al/rGO, Fe/rGO enhanced thermal conductivity of fluid more than single materials. Especially, the three-component materials Fe–Al/GO and Fe–Al/rGO have the highest thermal conductivity enhancement. Similar results were observed for Al_2O_3–MWCNT hybrid nanofluids (Nine et al. 2012), nanofluids of silver nanoparticles supported on silica (Hojjat et al. 2010), and Al_2O_3–CuO (Senthilraja et al. 2015) hybrid nanofluids. The heat transfer properties of silver nanoparticles decorated multiwalled carbon nanotubes–graphene mixture were investigated. An enhancement of ~ 8% in thermal conductivity is obtained for a volume fraction of 0.04% at 25 °C and the enhancement in heat transfer coefficient is about 570% for 0.005% volume fraction (Baby and Sundara 2013). The enhancement in thermal conductivity of hybrid nanofluids in this study could be due to high thermal conductivity of high surface area graphene, presence of high thermally conductive Al_2O_3 which acts as a connecting network between the graphene sheets, avoids the stacking of GO and rGO sheets, and increases the stability of GO and rGO in brine water. In addition, the addition of Fe_3O_4 with high thermal conductivity increases the overall thermal conductivity of the nanofluids and creates the magnetic properties for materials.

Evaluation of the thermal sorption capacity of materials

Evaluation the thermal absorption capacity of materials is carried out in the following steps: measuring the material's thermal absorption capacity, investigation of influence of material content and of light intensity on the material's thermal absorption capacity.

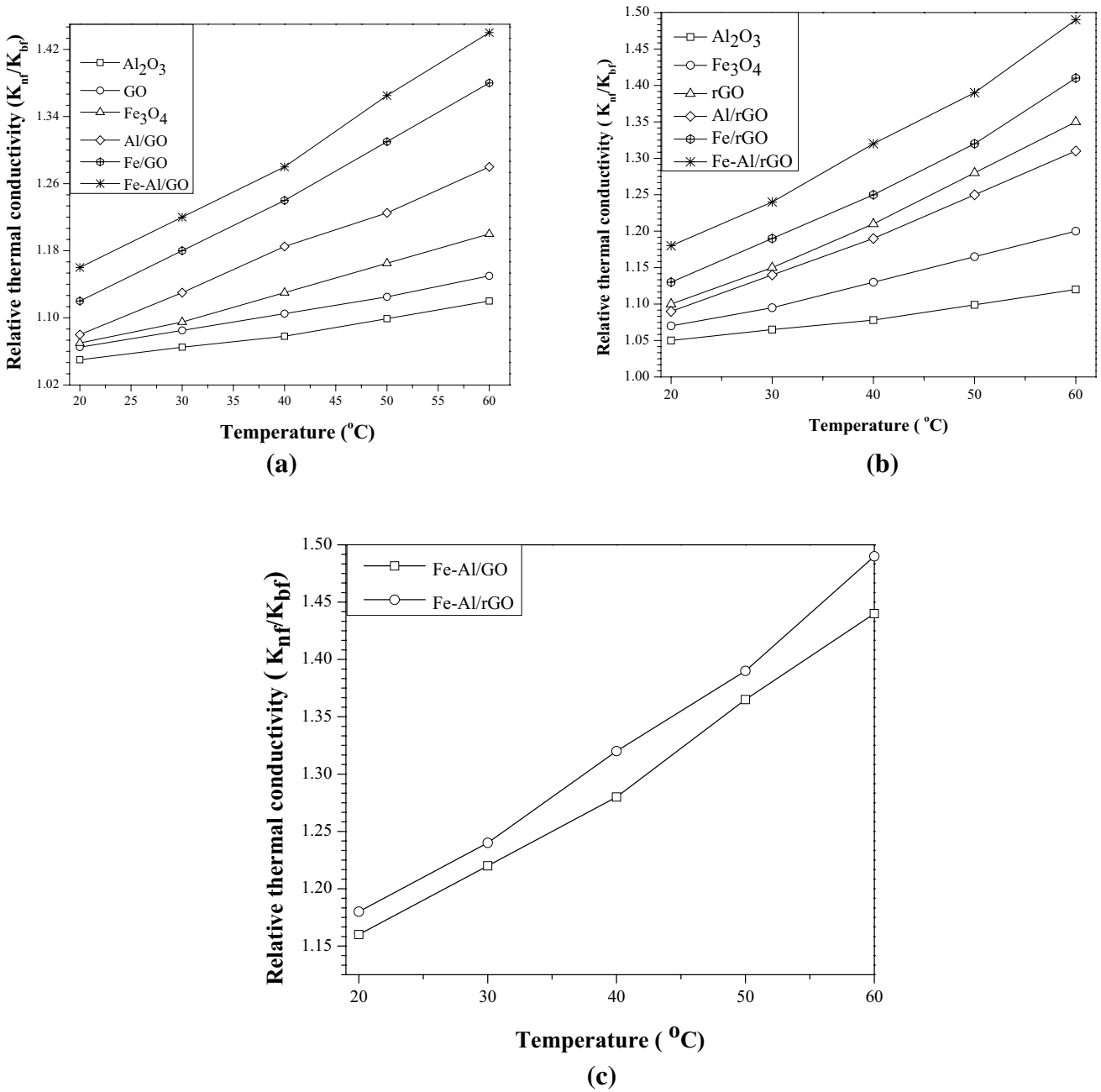

Fig. 10 The thermal conductivity enhancement of nanofluids of (**a**) GO-based materials and (**b**) rGO-based materials (**c**) of Fe–Al/GO and Fe–Al/rGO at 0.15 mg mL^{-1} in 3.5% NaCl aqueous solution

Thermal sorption capacity of different materials

To evaluate thermal absorption capacity of the prepared materials, these materials were dispersed into 3.5% NaCl aqueous solutions at a concentration of 0.15 mg mL^{-1}. Mixtures were lightened and their temperature and weights were measured periodically measured at different times for comparison. The variations of temperature enhancements and weight decreases of different materials with time are presented in detail in Fig. 11.

Results show that all studied materials could intensify the thermal absorption capacity of 3.5% NaCl aqueous solutions. The thermal absorption was enhanced due to the Brownian motion and collisions between nanoparticles in base fluids (Subelia et al. 2011). The thermal conductivity, transmittance spectrum of nanofluids and reflectance

spectrum of materials control reflect the thermal absorption of materials. Single Fe_3O_4 has high thermal absorption capacity (higher than singe GO and Al_2O_3) (Fig. 6a); this is ascribed to electron exchange between the Fe(II) and Fe(III) centers. It was found from the comparison of temperature of nanofluids GO, Al_2O_3 and Al/GO that the temperature of hybrid nanofluid of material Al/GO was higher than temperatures of single nanofluids of GO or Al_2O_3. Comparison of temperatures of GO, Fe_3O_4, and Fe/GO samples showed that the nanocomposite materials Al/GO also intensified the thermal absorption capacity of brine water more than single materials GO or Fe_3O_4. In particular, the composite Fe–Al/GO material has the highest thermal absorption capacity among GO-based materials; temperature rise of nanofluid containing this material was 7 °C higher than the blank sample.

The thermal sorption efficiency of rGO-based materials follows the order: blank sample < Al_2O_3 < Fe_3O_4 < Al/rGO < Fe/rGO < rGO < Fe–Al/GO. Single rGO has highest thermal sorption efficiency among single materials, much higher than GO, Al_2O_3 and Fe_3O_4. This is due to almost the oxygenated functional groups of GO were reduced during GO being transferred to rGO and almost C atoms of rGO are at sp^2 hybridization state and electrons are unlocalized. rGO is currently considered as one of the best conductive materials. But rGO is hydrophobic and its solution has low stability; rGO nanoparticles tend to agglomerate at high temperatures. When Al_2O_3 is combined with rGO, the conductivity of Al/rGO is higher than of Al_2O_3 but lower than rGO. Fe/rGO has higher thermal absorption capacity than single rGO or single Fe_3O_4 that has its own high thermal absorption capacity. In particular, the three-component composite material Fe–Al/rGO leaded to the highest thermal sorption; the temperature difference between investigated and blank samples is 8.5 °C. Magnetic nanocomposites based on graphene and carbon nanotubes also showed high thermal sorption than single materials (Stankovich 2007; Chen et al. 2019).

The decrease in weights of the nanofluids with different materials dispersed (0.15 mg mL^{-1} in 3.5% NaCl solution) was measured as functions of time. Similar to the change in temperature, the brine solution with Fe–Al/GO or Fe–Al/rGO dispersed has the highest evaporation mass loss in the two series of materials. The evaporation of nanofluids rises in range from 20% (with Al_2O_3 nanofluid) to 80% (with Fe–Al/rGO fluid) compared to brine water (Fig. 11c).

Influence of material content on thermal absorption of materials

Fe–Al/GO and Fe–Alr/GO showed higher thermal sorption capacity among two series of synthesized materials. Therefore, the influence of their concentration on thermal sorption capacity was investigated to determine the appropriate content dispersed in 3.5% NaCl solution. The temperature was periodically measured and recorded. The variations of temperature enhancements of materials with concentration and time are presented in detail in Fig. 12.

The temperature of solutions increased with increasing the content of nanoparticles dispersed in saline solution from 0.05 to 0.15 mg mL^{-1}. However, when the concentration of the nanoparticle increased to 0.2 mg mL^{-1} and the temperature is higher than 60 °C, the ability to absorb heat decreases. This can be due to high temperature and high nanoparticle concentration which lead to a high attraction between particles; they agglomerate to form larger particles and settle down, thus reducing the concentration of nanoparticles in nanofluids and, therefore, decrease the thermal conductivity and thermal sorption capacity of the system. The results showed that, at the concentration of 0.2 mg mL^{-1} of Fe–Al/GO, the sample has the highest thermal sorption ability. However, to save costs and reduce agglomeration for long periods, the concentration of nanoparticles in saline solution should be 0.10–0.15 mg mL^{-1} depending on the specific conditions.

Evaluation of the recovery and recycle ability of materials

Evaluation of the recovery ability of materials

During distillation, the evaporation of pure water and the introduction of seawater water happen simultaneously which result in the increase in concentration of salty water in still and the crystallization of salts. To dissolve the formed salt and begin new evaporation cycle, new seawater was added to the solution. After several cycles, high concentration solution became supersaturated. Then, the material needs to be recovered from the concentrated brine in order not to waste the materials. In order for the recovery process to occur quickly and completely, Fe_3O_4 nanoparticles were used together with GO (rGO) and Al_2O_3 to form magnetic materials. In addition, as seen in the previous sections, the introduction of magnetic Fe_3O_4 also creates a synergistic effect that enhances the material's thermal sorption ability.

When the system was allowed to naturally settle material recovery, the process was slow and incomplete; however, the material can be easily separated from a brine solution using an external magnetic during 5–7 min (Fig. 13). After decanting, washing, and drying, the recovery efficiency reached 98%.

Evaluation of the recycle ability of materials

The recovered nanoparticles was washed with clean water and dried, then was reused for new distillation. After five cycles (thermal sorption and recovery), the materials was

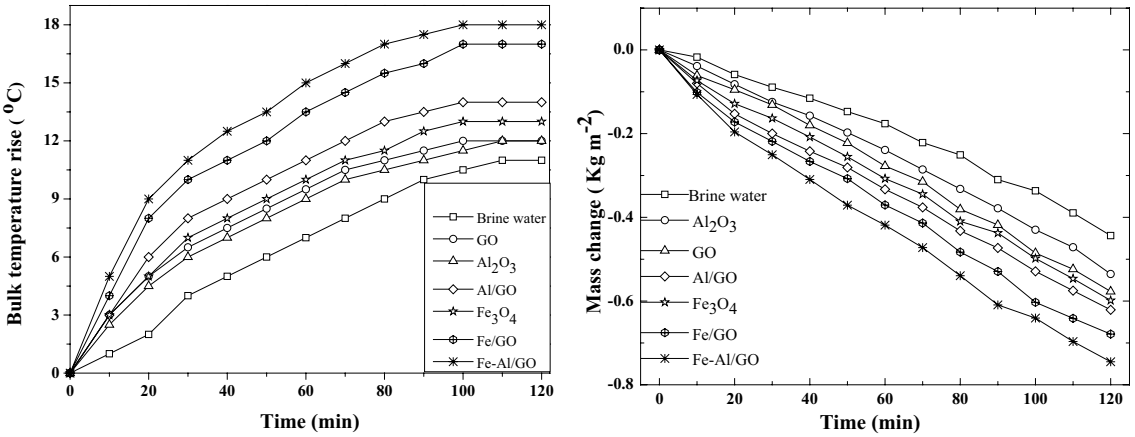

(a)

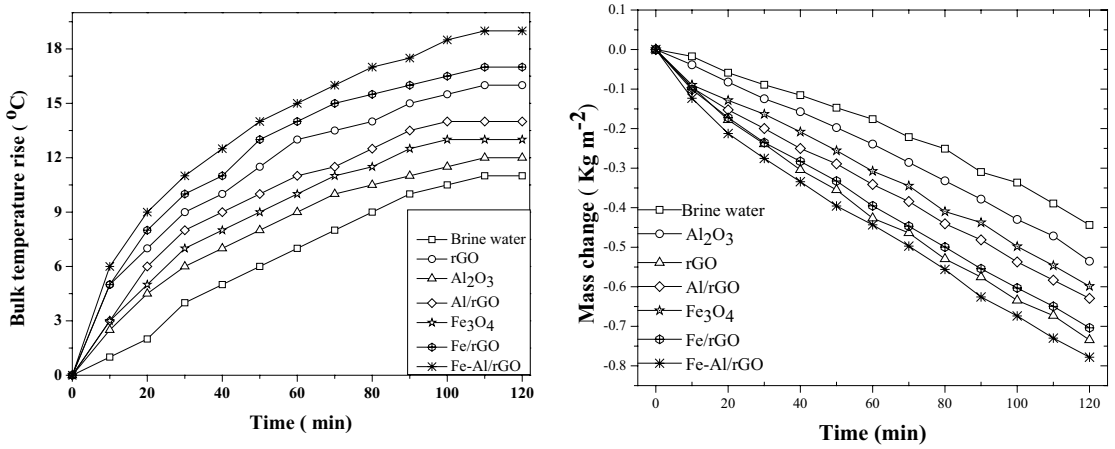

(b)

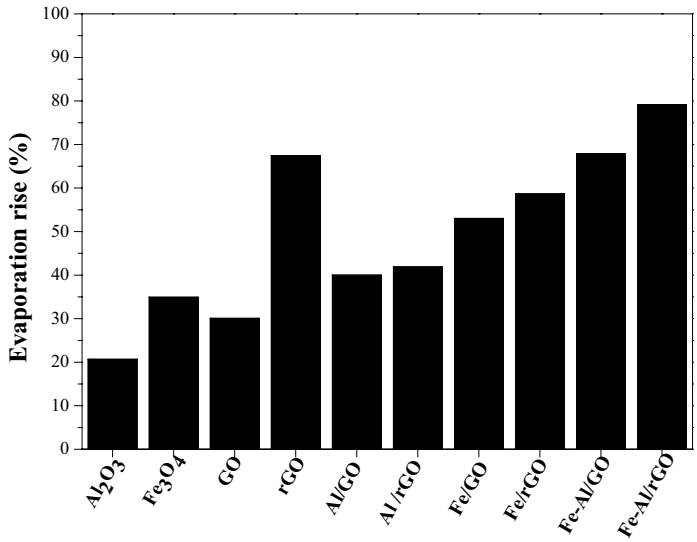

(c)

◂**Fig. 11** Evaporation performance of solutions containing nanomaterials. The bulk temperature rise profile and evaporation mass change of (**a**) saline water and GO-based materials and (**b**) saline water and rGO-based materials dispersed solution (0.15 mg mL^{-1} in 3.5% NaCl solution). The evaporation rise profile of nanofluids containing different nanoparticles (**c**)

analyzed by infrared spectrometry. Comparison of infrared images of the fresh and regenerated materials is shown in Fig. 14. The regenerated material has characteristic peaks similar to the peaks of the fresh material. This proves that there is no change in functional groups during the thermal sorption and recovering.

The thermal sorption abilities of fresh and regenerated materials (five cycles) were almost similar (Fig. 15). Only minor decrease in thermal sorption ability of regenerated material was observed. These results show the high recycled and reusable ability of prepared materials.

Distillation of brine water with the assistant of synthesized nanocomposite materials using solar energy

To demonstrate the practical application of nanocomposite materials in solar thermal water evaporation technology, distillation of brine water was conducted using solar energy with and without the assistant of synthesized nanocomposite materials in 4th June 2019 in Ha Noi. Similar to indoor experiments, the addition of Fe–Al/GO material significantly increased the thermal sorption ability of brine water. The temperature of the sample using Fe–Al/GO reached 54 °C, while the temperature of blank sample was 45 °C. 44 mL of fresh water was collected after 2 h from the sample using Fe–Al/GO material, while only 10 mL of fresh water was collected in the latter case. These results show the potential of using Fe–Al/GO material in the distillation of saline water to fresh water using solar energy.

Conclusion

GO- and rGO-based thermal sorption materials were successfully synthesized and characterized by FT-IR, X-ray, SEM, TEM, and EDX spectra. Results of transmittance spectra show that the darkness of materials controls incident light capture capacity of nanofluids. The nanofluids containing rGO or GO materials can capture 100% of incident light. It can be seen from reflectance spectra that Fe–Al/GO and Fe–Al/rGO absorbed more than 96% radiation of heat of light. Thermal conductivity of nanofluids depends on the structure and composition of synthesized materials and increases with increasing the concentration of nanoparticle and temperature of the fluids. Hybrid nanofluid showed high thermal conductivity than single nanofluids. These results are in agreement with thermal sorption ability evaluated by evaporation experiment of nanofluids.

Thermal sorption ability evaluation shows that all four single-component materials GO, rGO, Fe_3O_4, and Al_2O_3 can increase thermal sorption efficiency of brine water and almost composite materials give better efficiency than single materials. This could be explained by the combination of two or three components could create a synergy effect that would enhance the thermal sorption efficiency. In addition, Al_2O_3 could increase the dispersity ability of hydrophobic rGO in water. Both Fe_3O_4 and Al_2O_3 can enhance the thermal sorption efficiency of composite materials; Fe_3O_4 creates the magnetic property and Al_2O_3 helps to link components together to form composite materials that possessed more preeminent properties. Among investigated materials Fe–Al/GO and Fe–Al/rGO give higher sorption efficiency, the temperature differences between the brine water and nanofluids containing Fe–Al/GO and Fe–Al/rGO (0.15 mg mL^{-1}) are 7 °C and 8.5 °C, respectively. Influence of Fe–Al/GO concentration and lightening intensity on the material's thermal sorption ability were investigated. The results show that thermal sorption ability of Fe–Al/GO increased with the increasing of material concentration up 0.15 mg mL^{-1} and then decreased. The evaporation of nanofluids rises from 20 to 80% depending on concentration of nanoparticles.

The used material was easily recovered with a magnet with yield of 98% and the typical functional groups of recovered material had not changed and only minor decrease in thermal sorption ability was observed. The distillation of nanofluid using solar energy was accelerated by over four times when using Fe–Al/GO as thermal absorption agent.

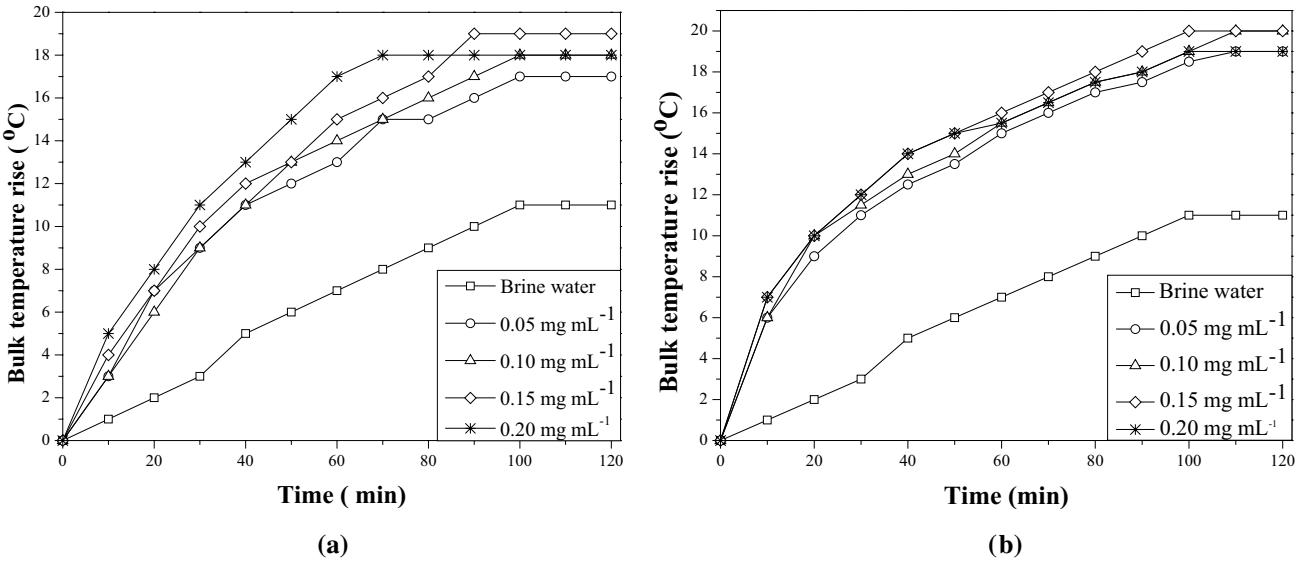

Fig. 12 Influence of (**a**) Fe–Al/GO and (**b**) Fe–Al/rGO concentration on the material's thermal absorption

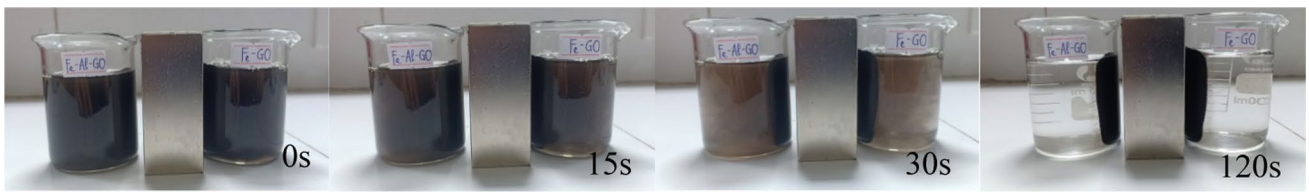

Fig. 13 Material sample Fe–Al/GO (left) and Fe/GO (right) (0.15 mg mL^{-1} in 3.5% NaCl solution) was settled with the magnet

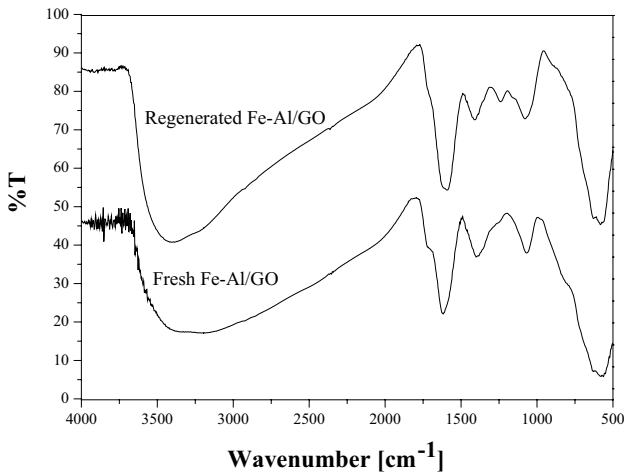

Fig. 14 Infrared spectrum of fresh and regenerated Fe–Al/GO

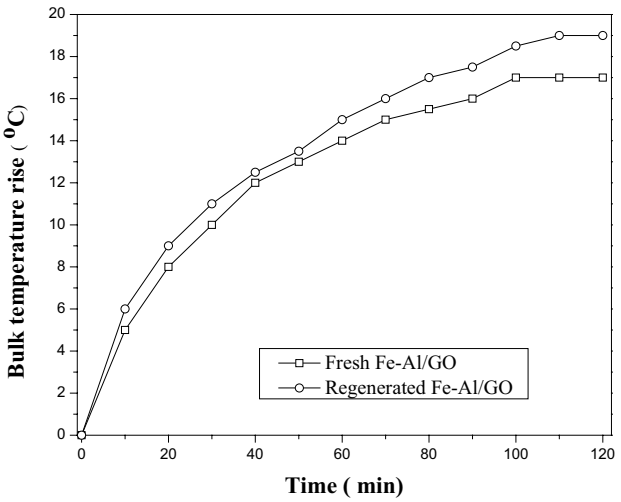

Fig. 15 Thermal sorption ability of regenerated (five cycles) and fresh material Fe–Al/GO (0.15 mg mL^{-1} in 3.5% NaCl solution)

Acknowledgments This work was supported by the Ministry of Education and Training, Viet Nam [B2019-MDA-01, 2019]

Compliance with ethical standards

Conflict of interest On behalf of all authors, the corresponding author states that there is no conflict of interest.

References

Al-harahsheh M, Abu-Arabi M, Mousa H, Alzghoul Z (2018) Solar desalination using solar still enhanced by external solar collector and PCM. Appl Therm Eng 128:1030–1040. https://doi.org/10.15866/ireme.v13i9.18006

Alibeyli R, Ata A, Topaç E (2014) Reduced graphene oxide synthesis via improved Hummers' method, ISITES 2014 Karabuk–Turkey, pp 650–660.

Amal AElS (2017) Performance of nanoparticle materials on radiation shieldingproperties using Mont Carlo method. Int J Eng Sci 6(6):74–82. https://doi.org/10.9790/1813-0606017482

Baby TT, Sundara R (2013) Synthesis of silver nanoparticle decorated multiwalled carbon nanotubes-graphene mixture and its heat transfer studies in nanofluid. API Adv, 3(1). doi: https://doi.org/10.1063/1.4789404.

Bartoluccia SF, Parasa J, Rafieeb MA, Rafieec J, Leea S, Kapoora D, Koratkarc N (2011) Graphene–aluminum nanocomposites. Mater Sci Eng A 528(27):7933–7937. https://doi.org/10.1016/j.msea.2011.07.043

Chen W, Zou C, Li X, Liang H (2019) Application of recoverable carbon nanotube nanofluids in solar desalination system: an experimental investigation. Desalination 451:92–101. https://doi.org/10.1016/j.desal.2017.09.025

Chen W, Zou C, Li X, Liang H (2017) Application of recoverable carbon nanotube nanofluids in solar desalination system: an experimental investigation. Desalination 451:92–1011. https://doi.org/10.1016/j.desal.2017.09.025

Elango T, Kannan A, Kalidasa Murugavel K (2015) Performance study on single basin single slope solar still with different water nanofluids. Desalination 360(45–51):16. https://doi.org/10.1016/j.desal.2015.01.004

El-Said EMS, Kabeel AE (2015) Theoretical study of a nanofluid solar collector assisted-hybrid desalination system for small communities need, Eighteenth International Water Technology Conference, IWTC18, Sharm ElSheikh.

Emad M-S, Kabeel AE, Abdulaziz M (2016) Theoretical study on hybrid desalination system coupled with nano-fluid solar heater for arid states. Desalination 386:84–98. https://doi.org/10.1016/j.desal.2016.03.001

Fugallo G, Cepellotti A, Paulatto L, Lazzeri M, Marzari N, Mauri F (2014) Thermal conductivity of graphene and graphite: collective excitations and mean free paths. Nano Lett 14:6109–6114. https://doi.org/10.1021/nl502059f

Hojjat M, Etemad SG, Bagheri R, Thibault J (2010) The thermal conductivity of non-Newtonian nanofluids. Int J Heat Mass Transf 54:1017–1023. https://doi.org/10.1016/j.ijheatmasstransfer.2010.11.039

Hu X, Yu Y, Zhou J, Wang Y, Liang J, Zhang X, Chang Q, Song L (2015) The improved oil/water separation performance of graphene oxidemodified Al_2O_3 microfiltration membrane. J Membr Sci 476:200–204. https://doi.org/10.1016/j.memsci.2014.11.043

International atomic energy agency. The world is thirsty. IAEA Division of Public Information (2012). https://www.iaea.org/newscenter/news/world-thirsty

Iqbal A, Sajjad S, Leghari SAK (2018) Low cost graphene oxide modified alumina nanocomposite as solar light induced photocatalyst. ACS Appl Nano Mater 1(9):4612–4621. https://doi.org/10.1021/acsanm.8b00649

Kanishka K, Silva HD, Huang HH, Yoshimura M (2018) Progress of reduction of graphene oxide by ascorbic acid. Appl Surf Sci 447:338–346. https://doi.org/10.1016/j.apsusc.2018.03.243

Madhesh D, Parameshwaran R, Kalaiselvam S (2014) Experimental investigation on convective heat transfer and rheological characteristics of Cu–TiO_2 hybrid nanofluids. Exp Thermal Fluid Sci 52:104–115. https://doi.org/10.1016/j.expthermflusci.2013.08.026

Madhu B, Bala Subramanian E, Nagarajan PK (2017) Improving the yield of freshwater and exergy analysis of conventional solar still with different nanofluids. FME Trans 45:524–530. https://doi.org/10.5937/fmet1704524M

Mahian O, Kianifar A, Heris SZ, Wen D, Shahin AZ, Wongwises S (2017) Nanofluids effects on the evaporation rate in a solar still equipped with a heat exchanger. Nano Energy 36:134–155. https://doi.org/10.1016/j.nanoen.2017.04.025

Mahmudul Haque AKM, Kwon S, Kim J, Noh J, Huh S, Chung H, Jeong H (2015) An experimental study on thermal characteristics of nanofluid with graphene and multi-wall carbon nanotubes. J Central South Univ 22:3202–3210. https://doi.org/10.1007/s11771-015-2857-3

Malega F, Indrayana IPT, Suharyadi E (2008) Synthesis and characterization of the microstructure and functional group bond of Fe_3O_4 nanoparticles form natural iron sand in Tobelo North Halmahera. J Ilmiah Pendidikan Fisika Al-BiRuNi 7:129–138. https://doi.org/10.24042/jipfalbiruni.v7i2.2913

Malega F, Indrayana PTI, Suharyadi E (2018) Synthesis and characterization of the microstructure and functional group bond of Fe_3O_4 nanoparticles form natural iron sand in Tobelo North Halmahera. J Ilmiah Pendidikan Fisika Al-BiRuNi 7:13–22. https://doi.org/10.24042/jipfalbiruni.v7i2.2913

Manimaran R, Palaniradja K, Alagumurthi N, Sendhilnathan S, Hussain J (2014) Preparation and characterization of copper oxide nanofluid for heat transfer applications. Appl Nanoscience 4:163–167. https://doi.org/10.1007/s13204-012-0184-7

Nine MJ, Batmunkh M, Kim J, Chung H, Jeong HM (2012) Investigation of Al_2O_3-MWCNTs hybrid dispersion in water and their thermal characterization. J Nanosci Nanotechnol 12(6):4553–4559. https://doi.org/10.1166/jnn.2012.6193

Ojeda JA, Messina S (2017) Enhancing energy harvest in a constructal solar collector by using alumina-water as nanofluid. Sol Energy 147:381–389. https://doi.org/10.1016/j.solener.2017.03.054

Patel Hrishikesh E, Sundararajan T, Das Sarit K (2010) An experimental investigation into the thermal conductivity enhancement in oxide and metallic nanofluids. J Nanopart Res 12:1015–1031. https://doi.org/10.1007/s11051-009-9658-2

Raj P, Subudhi S (2018) A review of studies using nanofluids in flat-plate and direct absorption solar collectors. Renew Sustain Energy Rev 84:54–74. https://doi.org/10.1016/j.rser.2017.10.012

Rogojan R, Andronescu E, Ghitulică C, Vasile BS (2011) Synthesis and characterization of alumina nano-powder obtained by sol-gel method. U.P.B. Sci. Bull, Ser B, 73(2).

Saram WS, Kazi SN, Badarudin A (2015) A review of studies using nanofluids in flat-plate and direct absorption solar collectors. Sol Energy 122:1245–1265. https://doi.org/10.1016/j.solener.2015.10.032

Selvakumar P, Suresh S (2012) Use of Al_2O_3-Cu/water hybrid nanofluid in an electronic heat sink. IEEE Trans Compon Pack Manuf Technol 2(10):1600–1607. https://doi.org/10.1109/TCPMT.2012.2211018

Senthilraja S, Vijayakumar K, Gangadevi R (2015) A comparative study on thermal conductivity of Al_2O_3/water, CuO/water and Al_2O_3–CuO/water nanofluids. Digest J Nanomater Biostruct, 10(4):1449–1458. http://www.chalcogen.ro/1449_Senthilraja.pdf

Shahriary L, Athawale AA (2014) Graphene oxide synthesized by using modified Hummers approach. Int J Renew Energy Environ Eng 2(1):58–63

Stankovich S, Dikin AD, Richard DP, Kohlhaas AK, Kleinhammes A, Jia Y, Wu Y, Nguyen TSB, Ruoff SR (2007) Synthesis of graphene–based nanosheets via chemical reduction of exfoliated graphite oxide. Carbon 45(7):1558–1565. https://doi.org/10.1016/j.carbon.2007.02.034

Subelia S, Botha PN, Bladergroen BJ (2011) Physicochemical properties of oil-based nanofluids containing hybrid structures of silver nanoparticles supported on silica. Ind Eng Chem Res 50(6):3071–3077. https://doi.org/10.1021/ie101088x

Suresh S, Venkitaraj KP, Selvakumar P, Chandrasekar M (2012) Effect of Al_2O_3–Cu/water hybrid nanofluid in heat transfer. Exp Thermal Fluid Sci 38:54–60. https://doi.org/10.1016/j.expthermflusci.2011.11.007

Syam Sundar L, Hashim Farooky Md, Naga Sarada S, Singh MK (2013) Experimental thermal conductivity of ethylene glycol and water mixture based low volume concentration of Al_2O_3 and CuO nanofluids. Int Commun Heat Mass Transfer 41:41–46. https://doi.org/10.1016/j.icheatmasstransfer.2012.11.004

Syam SL, Sharmab KV, Singha MK, Sousa AC (2017) Hybrid nanofluids preparation, thermal properties, heat transfer and friction factor: a review. Renew Sustain Energy Rev 68(1):185–198. https://doi.org/10.1016/j.rser.2016.09.108

Tawfik M, Tonnellier X, Sansoma C (2018) Light source selection for a solar simulator for thermal applications: a review. Renew Sustain Energy Rev 90:802–813

Varghese N, Hariharan M, Cherian AB, Sreenivasan PV, Paul J, Asmy AKA (2014) PVA—assisted synthesis and characterization of nano α -Alumina. Int J Sci Res Publ 4(10):1–5

Wang X, Ou G, Wang N, Wu H (2018) Graphene-based recyclable photo-absorbers for high-efficiency seawater desalination. ÁC Appl Mater Interfaces 8(14):9194–9199. https://doi.org/10.1021/acsami.6b02071

William S, Hummer J, Offerman RE (1958) Preparation of graphitic oxide. J Am Chem Soc 80:1339. https://doi.org/10.1021/ja01539a017

Zainuddin MF, Raikhan NHN, Othamn NH, Abullah WFH (2018) Synthesis of reduced graphene oxide (rGO) using different treatments of graphene oxide (GOIOP Conferenece Series: Materials Science and Engineering, 358, 3rd International Conference on Global Sustainability and Chemical Engineering (ICGSCE) 15–16 February 2017, Putrajaya, Malaysia. https://doi.org/https://doi.org/10.1088/1757-899X/358/1/012046

Zakaria I, Azmi WH, Mohamed WANW, Mamat R, Najafi G (2015) Experimental investigation of thermal conductivity and electrical conductivity of Al_2O_3 nanofluid in water—ethylene glycol mixture for proton exchange membrane fuel cell application. Int Commun Heat Mass Transfer 61:61–68. https://doi.org/10.1016/j.icheatmasstransfer.2014.12.015